WORKING FLUID SELECTION FOR ORGANIC RANKINE CYCLES BASED ON CONTINUOUS-MOLECULAR TARGETS

Johannes Schilling[1], Matthias Lampe[1], Joachim Gross[2], André Bardow[1*]

[1] Chair of Technical Thermodynamics, RWTH Aachen University,
Schinkelstraße 8, 52062 Aachen, Germany
E-mail: andre.bardow@ltt.rwth-aachen.de

[2] Institute of Thermodynamics and Thermal Process Engineering, Stuttgart University,
Pfaffenwaldring 9, 70569 Stuttgart, Germany

* Corresponding Author

ABSTRACT

Organic Rankine Cycles (ORCs) transform heat from low-temperature sources to electrical power. To ensure optimal use of a heat source, the cycle needs to be tailored to the specific application. Tailoring the cycle means optimizing both process and working fluid. Simultaneous optimization of process and working fluid is enabled by the Continuous-molecular targeting (CoMT) framework. Herein, working fluid properties are calculated by the perturbed-chain statistical associating fluid theory (PC-SAFT). The pure component parameters representing the working fluid are relaxed during the optimization leading to an efficient nonlinear program (NLP). The solution is an optimal combination of working fluid and process. Due to the relaxation, the pure component parameters of the optimal working fluid, in general, do not coincide with any real working fluid. Thus, real working fluids with similar properties are searched for in the following step, the so-called structure-mapping. Currently, a Taylor approximation of the objective function around the hypothetical optimal working fluid is used to estimate the objective function value of real working fluids. The Taylor approximation does not account for changes in the active set of constraints leading to occasional poor classification of the working fluids. To overcome this shortcoming, we present an adaptive structure-mapping: An additional Taylor approximation is added around a sampling point, if its approximation is poor. All Taylor approximations are combined using inverse distance weighting. The resulting adaptive structure-mapping improves the quality of the result and efficiently identifies the best working fluids. The approach is demonstrated in a case study for working fluid selection of a solar ORC.

1. INTRODUCTION

Organic Rankine Cycles enable the utilization of low-temperature heat to generate electrical power. Low-temperature heat is available from different sources, e.g., solar (Tchanche et al., 2009), geothermal (Heberle and Brüggemann, 2010), biomass (Drescher and Brüggemann, 2007) or waste heat (Wang et al., 2012). To ensure optimal use of a heat source, the cycle needs to be tailored to the specific application. For tailoring the cycle, both have to be optimized: process and working fluid.

Today, working fluid selection and process optimization are commonly carried out separately following a two-step approach (Tchanche et al., 2009; Drescher and Brüggemann, 2007; Quoilin et al., 2013): In a first step, working fluid candidates are preselected by experience and based on heuristic guidelines defining favorable working fluid properties. In the second step, the process is optimized for each preselected working fluid. For the preselection, a variety of different, partly conflicting heuristic criteria have been proposed. Papadopoulos et al. (2010) combine therefore computer-aided molecular design (CAMD) methods and multi-objective optimization for working fluid selection. Importantly, the proposed criteria can not reflect the actual operating conditions. However, if the heuristic knowledge underlying

the preselection fail, meaningful and promising working fluids are excluded leading to suboptimal solutions. Working fluid selection is inherently coupled to process optimization. Thus, recent reviews (Quoilin et al., 2013; Bao, J. and Zhao, L., 2013) recommend including working fluid selection in process optimization to obtain an overall optimal solution. However, the direct integration of these two design tasks leads to a mixed integer nonlinear program (MINLP) of prohibitive size and complexity for practical applications (Lampe et al., 2014). Recently, Papadopoulos et al. (2013) use a process-related objective function. The working fluid properties are modeled by a cubic equation of state and combined with a process model.

Simultaneous optimization of process and working fluid is achieved in the Continuous-molecular targeting framework by relaxation of the pure component parameters describing the working fluid (Bardow et al., 2010; Lampe et al., 2014; Stavrou et al., 2014). Here, in a first step, a hypothetical working fluid is identified maximizing a process-based objective function. Then, real working fluids with similar properties are identified in the second step, the so-called structure-mapping. For this purpose, a Taylor approximation around the hypothetical optimal working fluid is used to estimate the objective function value of real working fluids. However, this local approximation suffers from occasional poor classification of real working fluids. In this work, we present a method for adaptive structure-mapping to allow for efficient identification of the best working fluids.

The paper is structured as follows: in section 2, the current CoMT framework is briefly reviewed. Our method for adaptive structure-mapping is introduced in section 3. In section 4, the adaptive structure-mapping is applied to a case study and the results are analyzed. Conclusions are drawn in section 5.

2. CONTINUOUS-MOLECULAR TARGETING FRAMEWORK

Selecting a suitable working fluid is a generic problem with applications beyond ORC processes. Bardow et al. (2010) propose a generic approach, the so-called continuous-molecular targeting (CoMT). The approach was first applied to achieve simultaneous optimization of solvents and processes. Lampe et al. (2014) successfully applied the CoMT framework for the simultaneous process and working fluid optimization of ORC processes (Figure 1).

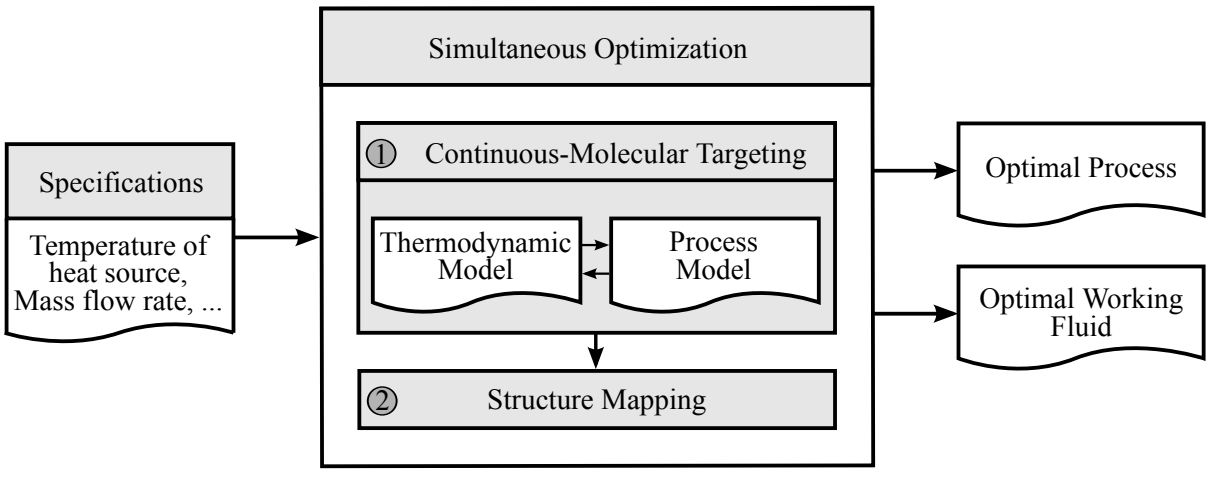

Figure 1: Simultaneous optimization of working fluid and process using the CoMT framework

To allow for the integrated process and working fluid optimization, we exploit the rich molecular picture underlying the perturbed-chain statistical associating fluid theory (PC-SAFT) equation of state (Gross and Sadowski, 2001). PC-SAFT is a model of the Helmholtz energy, which ensures a consistent picture of all equilibrium properties of the working fluid. A set of typically up to seven pure component parameters describes each working fluid (Stavrou et al., 2014). For simplicity, non-polar and non-associative

working fluids are considered in this work. Each working fluid is then described by three parameters: the segment number m, the segment diameter σ, and the segment dispersion energy ϵ/k.
A direct formulation of the integrated optimization using the pure component parameters as variables leads to a MINLP of prohibitive size and complexity, because a discrete degree of freedom is added to the problem for each real working fluid. Here, the MINLP is avoided by relaxing the pure component parameters during the simultaneous optimization of process and working fluid. Relaxation transforms the MINLP into a NLP of the form

$$\begin{aligned} &\max_{x,y} f(x,y) \\ s.t.\quad &g(x,y) \leq 0 \\ &h(x,y) = 0 \\ &Ay \leq b \\ &x_{\text{min}} \leq x \leq x_{\text{max}} \ \in \mathrm{R}^{\mathrm{n}} \\ &y_{\text{min}} \leq y \leq y_{\text{max}} \ \in \mathrm{R}^{\mathrm{m}} \end{aligned} \tag{1}$$

where x denotes the process variables, y denotes the pure component parameters and $f(x,y)$ denotes the objective function to be optimized. Here, any objective function can be employed, which is based on equilibrium thermodynamics. First approaches are available to even calculate transport properties based on PC-SAFT (Novak, 2011; Lötgering-Lin and Gross, 2015). The integration of such approaches would allow for a thermoeconomic objective function still requiring only PC-SAFT parameters to describe the working fluid. Without loss of generality, maximization is considered. The inequality and equality constraints of the process as well as PC-SAFT are formed by $g(x,y)$ and $h(x,y)$. The solution of Problem (1) is a hypothetical optimal working fluid y^* and the corresponding optimal process parameters x^*. In general, the hypothetical optimal working fluid does not coincide with a real fluid. To identify real fluids, a database of pure component parameters is used in this work. The values of the database can, in turn, be used to constrain the search space for optimization. For this purpose, a convex hull around the pure component parameters of real working fluids y_{k} of a database is used. The convex hull is represented by the set of linear constraints $Ay \leq b$ in Problem (1).
In the second step, real working fluids with similar properties as the hypothetical optimal working fluid are identified (Figure 1). Currently, a second degree Taylor approximation around the hypothetical optimal working fluid is used to estimate the objective function value of real working fluids (Bardow et al., 2010; Lampe et al., 2014; Stavrou et al., 2014). For this purpose, it is necessary to rewrite the objective function $f(x,y)$ as

$$\begin{aligned} \tilde{f}(y) \ = \ &\max_{x} f(x,y) \\ &s.t.\quad g(x,y) \leq 0 \\ &\qquad h(x,y) = 0 \\ &\qquad x_{\text{min}} \leq x \leq x_{\text{max}} \ \in \mathrm{R}^{\mathrm{n}}. \end{aligned} \tag{2}$$

From Problem (2), the Taylor approximation around optimum values y^* is calculated:

$$T(y) = \tilde{f}(y^*) + J(y^*)(y-y^*) + \frac{1}{2}(y-y^*)^{\mathrm{T}} H(y^*)(y-y^*). \tag{3}$$

Here, $J(y^*)$ denotes the Jacobian and $H(y^*)$ the Hessian of $\tilde{f}(y)$ at the sampling point y^*. Thus, the approximation of the performance for a working fluid is solely characterized by pure component parameters y_k. Based on the approximation $T(y_{\text{k}})$, a ranking of potential working fluids is obtained. Each working fluid is classified by the rank r of the ranking. However, the Taylor approximation does not account for changes in the active set of constraints (Lampe et al., 2014), whereby a substantial deviation between the Taylor approximation and the real objective function value occurs (Figure 2a). Thus, working fluids are classified wrongly. To overcome these shortcomings, an adaptive structure-mapping is presented.

3. ADAPTIVE STRUCTURE-MAPPING

The adaptive structure-mapping iteratively identifies sampling points to adapt the approximation. In section 3.1, the method for selection of additional sampling points is presented. The adaption of the current approximation is detailed in section 3.2.

3.1 Algorithm

The key idea for the adaption of approximation is to apply a Taylor approximation not only once at the hypothetical optimal working fluid, but also at additional sampling points. The individual Taylor approximations $T_{\mathrm{i}}(y)$ are combined to an adapted approximation $A(y)$ (Figure 2). The sampling points are selected in regions with a substantial deviation between the current approximation and the objective function. Through an iterative selection of suitable sampling points, the approximation, and therefore the structure-mapping, is adapted until a sufficient accuracy is achieved.

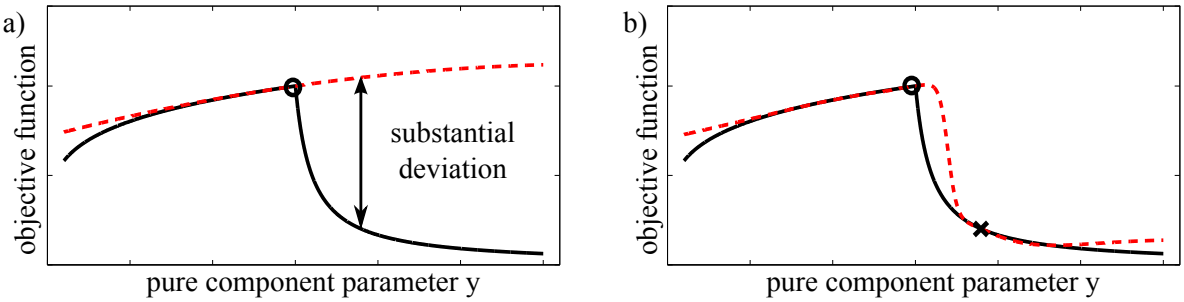

Figure 2: Qualitative illustration of the adapted approximation of the objective function $\tilde{f}(y)$ (black, solid) in the mapping step: a) Taylor approximation $T(y)$ (red, dashed) around the optimum y^* (marker ○), b) adapted approximation $A(y)$ (red, dashed) with an additional sampling point (marker ×) in a region with previous substantial deviation between the objective function and the approximation.

The starting point is the ranking based on the Taylor approximation around the hypothetical optimal working fluid (step 1 in Figure 3). The selection of the next sampling point is performed by a systematic analysis of the current ranking (step 2). Beginning with the highest ranked working fluid $r = 1$ and following the order of the ranking , the real objective function value $\tilde{f}(y_{\mathrm{r}})$ of the r-th ranked working fluid y_{r} is calculated from Problem (2) (step 2a). This procedure continues, until the absolute difference ΔA_{r} between approximation $A(y_{\mathrm{r}})$ and real objective function value $\tilde{f}(y_{\mathrm{r}})$ exceeds a threshold ΔA_{max} (step 2b)

$$\Delta A_{\mathrm{r}} = |A(y_{\mathrm{r}}) - \tilde{f}(y_{\mathrm{r}})| > \Delta A_{\mathrm{max}}. \tag{4}$$

Here, r denotes the rank of the working fluid in the current ranking. In this work, the threshold ΔA_{max} is set to $5\,\%$ of the objective function value of the hypothetical optimal working fluid. If the absolute difference ΔA_{r} exceeds the threshold, the pure component parameters of this r-th ranked working fluid are selected as additional sampling point. The approximation $A(y)$ is adapted by taking a Taylor approximation of the additional sampling point into account (step 3, see section 3.2 for details). A revised ranking of potential working fluids is obtained based on the adapted approximation (step 4). Subsequently, a termination criterion is checked (step 5). The algorithm stops, if for the first 15 ranks of the revised ranking a process optimization is performed in a previous iteration. If the termination criterion is not fulfilled, the algorithm continues at step 2. Beginning with the highest ranked working fluid $r = 1$, the algorithm analyzes the revised ranking systematically to select one more additional sampling point. Thus, the approximation is iteratively adapted to the objective function, since a region with previous poor approximation is improved by an additional Taylor approximation in each iteration. As a result, the method yields a ranking based on the real objective function values of the already calculated working fluids and the approximations of all further working fluids. The adaptive structure-mapping improves the quality of the ranking and allows for efficient identification of the best working fluids.

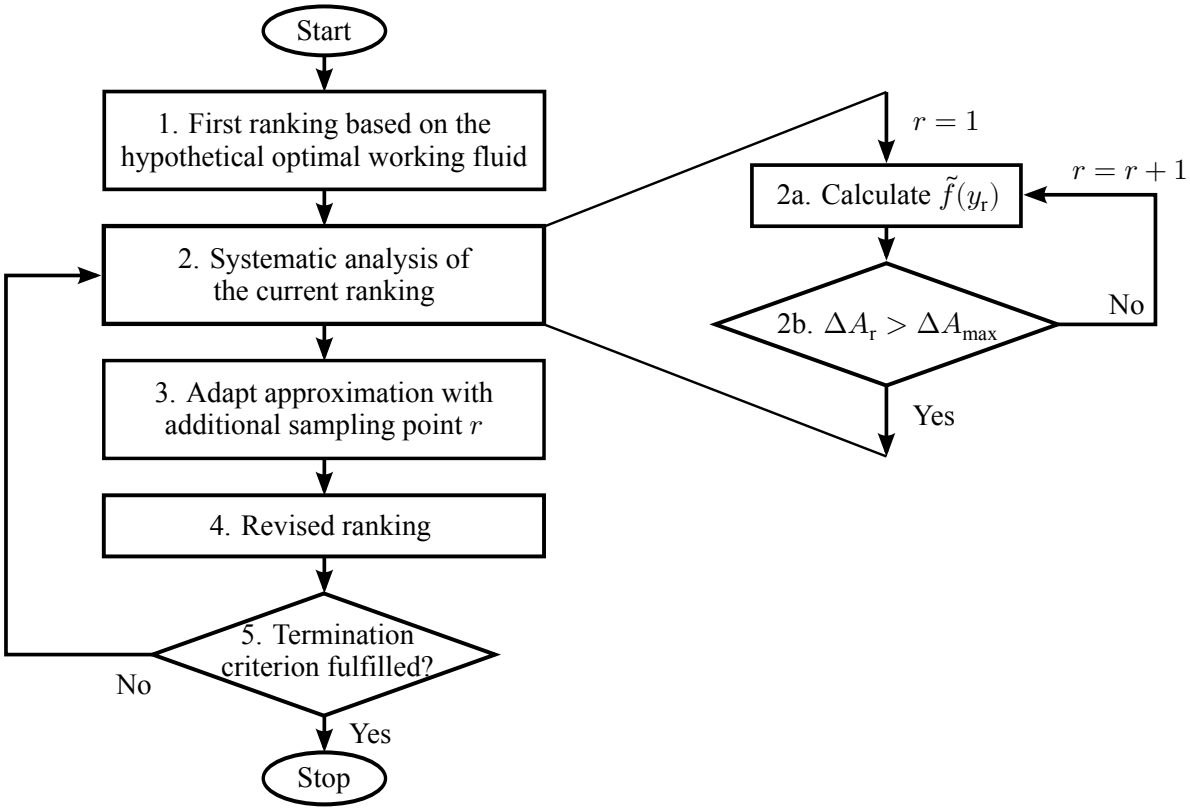

Figure 3: Flow chart for adaptive structure-mapping.

3.2 Adaptive approximation

The adaptive approximation $A(y)$ is a weighted sum of individual Taylor approximations $T_i(y)$. The Taylor approximations $T_i(y)$ are calculated by Equation (3), whereby the pure component parameters of the hypothetical optimal working fluid y^* are replaced by the sampling points y_i. The individual Taylor approximations $T_i(y)$ around the sampling points y_i are multiplied by a weighting factor $w_i^*(y)$ and combined to an adapted overall approximation $A(y)$ of the objective function

$$A(y) = \sum_{i=1}^{S} w_i^*(y) \cdot T_i(y), \tag{5}$$

whereby S denotes the number of sampling points. The weighting factor $w_i^*(y)$ increases the influence of Taylor approximation $T_i(y)$ the closer the pure component parameters y are to the corresponding sampling point y_i. A suitable method for this purpose is the so-called inverse distance weighting. In this work, the distance between two points in the three-dimensional space spanned by the pure component parameters $y = (m, \sigma, \epsilon/k)^T$ is considered. The pure component parameters have different magnitudes and units. To prevent effects of different scaling, the pure component parameters are normalized to one by

$$m_n = \frac{m - m_{min}}{m_{max} - m_{min}}, \quad \sigma_n = \frac{\sigma - \sigma_{min}}{\sigma_{max} - \sigma_{min}}, \quad (\epsilon/k)_n = \frac{(\epsilon/k) - (\epsilon/k)_{min}}{(\epsilon/k)_{max} - (\epsilon/k)_{min}}, \tag{6}$$

yielding normalized pure component parameters $y_n = (m_n, \sigma_n, (\epsilon/k)_n)^T$. Here, parameters $y_{j,min}$ and $y_{j,max}$ are the smallest and largest value of the pure component parameters of the database respectively. The inverse distance $d_i^p(y)$ of the Taylor approximation $T_i(y)$ around a sampling point y_i is calculated by (Dumitru et al., 2013):

$$d_i^p(y) = \frac{1}{\|y_n - y_{n,i}\|^p}. \tag{7}$$

The weighting factor depends on the so-called power parameter p. The best results are typically obtained for $p = 2$ (Dumitru et al., 2013). To ensure that the approximation at the sampling point matches the

objective function value, the sum of all inverse distances is normalized to one leading to a weighting factor $w_{\mathrm{i}}^{*}(y)$:

$$w_{\mathrm{i}}^{*}(y) = \frac{d_{\mathrm{i}}^{-p}(y)}{\sum_{\mathrm{u}=1}^{S} d_{\mathrm{u}}^{-p}(y)}. \tag{8}$$

The approximation $A(y)$ does not explicitly account for changes in the active set of constraints. However, the adaption captures the behavior of the objective due to the changes in the active set.

The adaptive approximation improves the solution but it can also produce suspicious solution as shown in the following. Figure 4 illustrates a qualitative one-dimensional example for the objective function and its approximation. A second degree Taylor approximation around a sampling point in a region with strong convex curvature leads to unphysical approximation and slow convergence of the adaptive structure-mapping (Figure 4a). This difficulty is circumvented by using a first degree Taylor approximation instead of a second degree Taylor approximation in regions with convex curvature (Figure 4b).

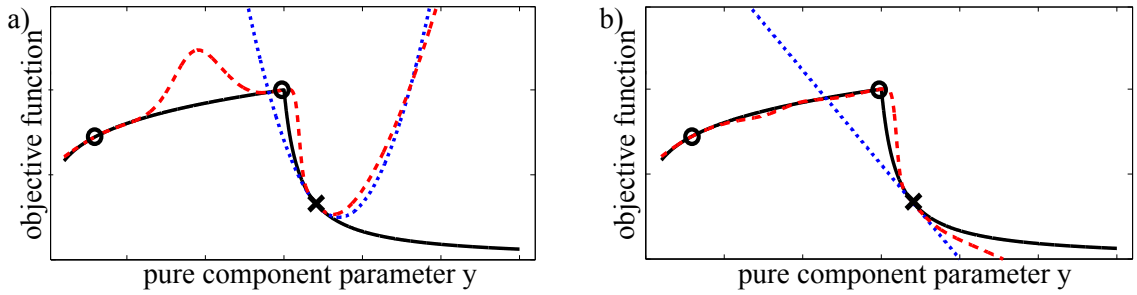

Figure 4: Approximation $A(y)$ (red, dashed) of the objective function $\tilde{f}(y)$ (black, solid) with a) second degree and b) first degree Taylor approximation $T_{\mathrm{i}}(y)$ (blue, dotted) around a sampling point in a region with strong convex curvature (marker ×)

In the multidimensional case, a function is considered to be concave, if a concave curvature exists in all spatial directions. In the major part of the considered parameter space, the objective function shows both concave and convex curvatures in the various spatial directions. If first degree Taylor approximations are used whenever one spatial direction has convex curvature, a first degree Taylor approximation is chosen for almost all sampling points. This leads to slow convergence of the adaptive structure-mapping and, thus, longer computing time, since the approximation is much less accurate.
For this reason, we classify the vicinity of a sampling point as concave, if possible convex curvatures in all directions are negligible compared to the concave curvature. Curvature is evaluated from the eigenvalues of the Hessian $\tilde{H}(y_{\mathrm{i}})$ of the objective function $\tilde{f}(y)$. In order to ensure comparability of the eigenvalues, the Hessian is transformed to the normalized parameter space (Equation (6)). Positive eigenvalues characterize convex and negative concave curvature; the magnitude is a measure for the strength of the curvature. We allow convex curvature, if the highest eigenvalue λ_{max} of the normalized Hessian is at least an order of magnitude smaller than the amount of the lowest eigenvalue λ_{min}. With this restriction, the Hessian $H(y_{\mathrm{i}})$ in Equation (3) is

$$H(y_{\mathrm{i}}) = \begin{cases} \tilde{H}(y_{\mathrm{i}}), & \text{if } \; 10 \cdot \lambda_{\mathrm{max}} < |\lambda_{\mathrm{min}}| \\ 0_{3,3}, & \text{otherwise.} \end{cases} \tag{9}$$

Using this heuristic, more second degree Taylor approximations are selected, while avoiding unphysical impact of the convex curvature. This curvature approach proves suitable in all case studies.

4. CASE STUDY – SMALL-SCALE SOLAR THERMAL ORC SYSTEM

The adaptive structure-mapping is applied to the optimization of a ORC process with direct solar evaporation based on Casati et al. (2011). A recuperator is used to increase the efficiency. The net power

output P_{net} is considered as objective function. The degrees of freedom in the process model are: pressure of the condenser p_{cond}, pressure of the evaporator p_{evap}, degree of superheating ΔT_{sh} and mass flow rate of the working fluid $\dot{m}_{\text{wf}}$. We assume a fixed heat flow of the solar field $\dot{Q}_{\text{solar}}$ at the temperature T_{Q} (Table 1). A minimal temperature difference in the heat exchangers ΔT_{pinch} is imposed to ensure feasible heat transfer. The pressure levels in the cycle are further constrained by minimal and maximal absolute pressures p_{min} and p_{max}, respectively.

Table 1: Solar source specifications and constraints for the case study

Parameter	Symbol	Value
temperature of heat source	T_{Q}	380 °C
heat flow of the solar field	$\dot{Q}_{\text{solar}}$	463 kW
temperature of heat sink	T_{S}	80 °C
maximal absolute pressure	p_{max}	50 bar
minimal absolute pressure	p_{min}	0.05 bar
minimal temperature difference	ΔT_{pinch}	10 K
isentropic turbine efficiency	η_{T}	80 %
generator efficiency	η_{G}	95 %
isentropic pump efficiency	η_{P}	70 %
mechanic pump efficiency	$\eta_{\text{P,mech}}$	90 %

The adaptive structure-mapping is applied to a database of 223 working fluids. In order to evaluate the results of the structure-mapping, an individual process optimization for all working fluids of the database is performed. A real ranking is obtained, which serves as an unambiguous measure for the quality of the ranking from the adaptive structure-mapping. Thus, the database is comparatively small to allow for an efficient validation. The database can easily be extended to consider more fluids. Alternatively, computer-aided molecular design can be employed for the design of working fluids (Lampe et al., 2015). For this case study, the adaptive structure-mapping terminates after two iterations, i.e., three sampling points are used for the overall approximation. All sampling points are approximated by a second degree Taylor approximation. To evaluate the results of the adaptive structure-mapping, the ranking after each iteration is compared to the real ranking. Spearman's rank correlation coefficient ρ_{s} serves as a measure for the correlation (Puth et al., 2015): The closer the correlation coefficient ρ_{s} is to one, the better is the correlation. The corresponding real rank is plotted for the 60 highest ranked working fluids of the structure-mapping (Figure 5).

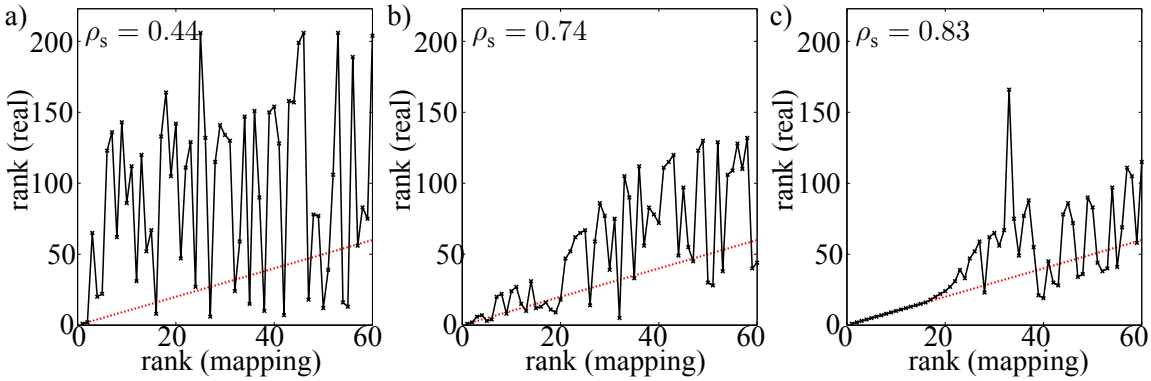

Figure 5: Comparison of result of the CoMT-CAMD approach (black, solid) with one (a), two (b) and three (c) sampling points and the ideal result (red, dotted)

The original structure-mapping with only one Taylor approximation around the hypothetical optimal working fluid identifies the best two working fluids but shows large deficits (Figure 5a): Many working fluids are overestimated and ranked too well. Here, Spearman's rank correlation coefficient is $\rho_{\text{s}} = 0.44$.

The result with two sampling points shows a better correlation ($\rho_s = 0.74$, Figure 5b). In particular, the top 20 are already well captured. The final result with three sampling points identifies the top 20 nearly in the correct order ($\rho_s = 0.83$, Figure 5c).

The original structure-mapping with one Taylor approximation around the hypothetical optimal working fluid identifies only 2 working fluids of the top 10 (4 of the top 20). This result is improved significantly by the adaptive structure-mapping: all working fluids of the top 10 and 18 of the top 20 are identified correctly. The improvement is archived by a more accurate approximation of the objective function in the relevant region. To visualize the functionality of the adaptive structure-mapping, the working fluid ethylcyclohexane is examined ($m = 3.0$, $\sigma = 4.0\,\text{Å}$, $\epsilon/k = 283.8\,\text{K}$). Ethylcyclohexane is ranked 9th in the real ranking. Figure 6 shows the optimal net power output $\tilde{f}$ as function of the segment number m for constant segment diameter σ and segment dispersion energy ϵ/k corresponding to the pure component parameters of ethylcyclohexane. The pure component parameters of the hypothetical optimal working fluid y^* are $m^* = 1.8$, $\sigma^* = 4.1\,\text{Å}$, and $(\epsilon/k)^* = 408.6\,\text{K}$ and are not in the plane of Figure 6. Additionally, the approximation function $A(y)$ with one, two, and three sampling points are plotted. The Taylor approximation around the optimum is not sufficient to approximate the objective function in this region. A substantial deviation between the approximation $A(y)$ and the objective function $\tilde{f}(y)$ occurs: ethylcyclohexane is underestimated and ranked 69th. However, the approximation with three sampling points corresponds well to the objective function. Ethylcyclohexane is correctly ranked 9th in the final ranking.

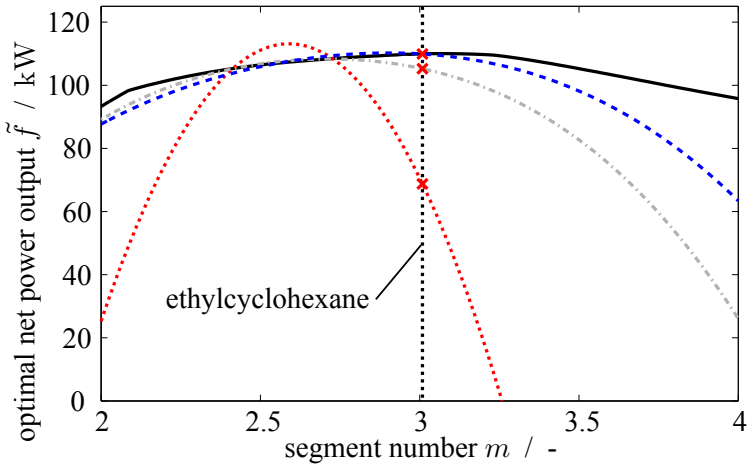

Figure 6: Optimal net power output $\tilde{f}$ (black, solid) and the approximation function $A(y)$ with one (red, dotted), two (gray, dash-dotted) and three (blue, dashed) sampling points as function of the segment number m for constant segment diameter $\sigma = 4.0\,\text{Å}$ and segment dispersion energy $\epsilon/k = 283.8\,\text{K}$ corresponding to the pure component parameters of ethylcyclohexane. The optimal values are $m^* = 1.8$, $\sigma^* = 4.1\,\text{Å}$ and $(\epsilon/k)^* = 408.6\,\text{K}$.

Finally, the effectiveness of the method is evaluated based on the required computing effort. The number of function evaluations of the objective function in the optimizations for both the adaptive structure-mapping and the calculation of the real ranking are compared. For the adaptive structure-mapping, the function evaluations of the CoMT-optimization, the calculation of Jacobians and Hessians by finite differences, and the calculation of real objective function values are considered. For the real ranking, the function evaluations to calculate the individual process optimizations of each working fluid of the database are counted.

The calculation of the real ranking requires 31,537 function evaluations. The calculation of the case study by the adaptive structure-mapping takes 3,951 function evaluations, which corresponds to savings of 87.5 %. Thus, the adapted CoMT framework is far more efficient than an individual optimization of each working fluid to identify the best working fluids. Considering a larger database, the number

of function evaluations to calculate the real ranking would increase with the number of working fluids. In contrast, in our experience, there is no direct correlation between the number of working fluids and function evaluations in the CoMT framework, so that overall, the efficiency of the CoMT framework is expected to increase.
If the heuristic regarding the negligible convex curvature is not made (see Section 3.2), the adapted CoMT framework requires $12{,}805$ function evaluations and 10 sampling points to identify the ten best working fluids. In this case, five first degree Taylor approximations and five second degree Taylor approximations are employed. If exclusively first degree polynomials are used, the CoMT framework requires $17{,}838$ function evaluations and 24 sampling points. The results demonstrate the advantage of using second degree polynomials and the heuristic regarding negligible convex curvature.

5. CONCLUSIONS

Simultaneous design of ORC process and working fluid is enabled by the Continuous-molecular targeting framework. However, mapping of the targets onto real working fluids occasionally failed. For this purpose, an adaptive structure-mapping is presented to identify the best working fluids for ORC processes based on continuous-molecular targets. The approximation used for the structure-mapping is iteratively adapted by combining several Taylor approximations around different sampling points. A method to select sampling points is presented and a heuristic for the selection of the degree of the Taylor approximations is proposed. The result of the method is a ranked set of working fluids. The adaptive structure-mapping improves the quality of the ranking and allows for efficient identification of the best working fluids.
The adaptive structure-mapping is successfully applied to a case study, where the original mapping only identifies 2 working fluids out of the top 10 correctly. The adaptive method correctly identifies all working fluids of the top 10. Thereby, the adaptive structure-mapping is more efficient than an individual optimization of each working fluid: In this case study, the function evaluations are reduced by $87.5\,\%$.

NOMENCLATURE

A	approximation function	(-)	T	Taylor approximation	(-)
d^{-p}	inverse distance	(-)	w^*	normalized weighting factor	(-)
f, $\tilde{f}$	objective function	(-)	x	process variables	(-)
g	inequality constraints	(-)	x^*	optimal process parameters of y^*	(-)
H, $\tilde{H}$	Hessian	(-)	y	pure component parameters	(-)
h	equality constraints	(-)	y^*	hypothetical optimal working fluid	(-)
J	Jacobian	(-)	ϵ/k	associating energy	(K)
m	segment number	(-)	λ	eigenvalues	(-)
p	power parameter	(-)	ρ_s	rank correlation coefficient	(-)
S	number of sampling points	(-)	σ	segment diameter	(Å)

Subscript

i	sampling point	min	minimal
k	real working fluid of the database	n	normalized
max	maximal	r	rank

REFERENCES

Bao, J. and Zhao, L. (2013). A review of working fluid and expander selections for organic rankine cycle. *Renewable and Sustainable Energy Reviews*, 24:325–342.

Bardow, A., Steur, K., and Gross, J. (2010). Continuous-molecular targeting for integrated solvent and process design. *Ind. Eng. Chem. Res.*, 49(6):2834–2840.

Casati, E., Colonna, P., and Nannan, N. R. (2011). Supercritical ORC turbogenerators coupled with linear solar collectors. In *Proceedings of the ISES solar world congress 2011, Kassel, Germany, 2011*.

Drescher, U. and Brüggemann, D. (2007). Fluid selection for the organic rankine cycle (ORC) in biomass power and heat plants. *Applied Thermal Engineering*, 27(1):223 – 228.

Dumitru, P. D., Plopeanu, M., and Badea, D. (2013). Comparative study regarding the methods of interpolation. In *1st European Conference of Geodesy & Geomatics Engineering 2013, Recent Advanced in Geodesy and Geomatics Engineering–Conference Proceedings, 45-52pp, Antalya, Oct. 8*, volume 10.

Gross, J. and Sadowski, G. (2001). Perturbed-chain SAFT: An equation of state based on a perturbation theory for chain molecules. *Ind. Eng. Chem. Res.*, 40(4):1244–1260.

Heberle, F. and Brüggemann, D. (2010). Exergy based fluid selection for a geothermal organic rankine cycle for combined heat and power generation. *Applied Thermal Engineering*, 30(11-12):1326 – 1332.

Lampe, M., Stavrou, M., Bücker, H. M., Gross, J., and Bardow, A. (2014). Simultaneous optimization of working fluid and process for organic rankine cycles using PC-SAFT. *Ind. Eng. Chem. Res.*, 53(21):8821–8830.

Lampe, M., Stavrou, M., Schilling, J., Sauer, E., Gross, J., and Bardow, A. (2015). Computer-aided molecular design in the continuous-molecular targeting framework using group-contribution PC-SAFT. *Computers & Chemical Engineering*.

Lötgering-Lin, O. and Gross, J. (2015). A group contribution method for viscosities based on entropy scaling using the perturbed-chain polar statistical associating fluid theory. *Ind. Eng. Chem. Res.*, submitted.

Novak, L. T. (2011). Fluid viscosity-residual entropy correlation. *Int. J. Chem. React. Eng.*, 9(1).

Papadopoulos, A. I., Stijepovic, M., and Linke, P. (2010). On the systematic design and selection of optimal working fluids for organic rankine cycles. *Applied Thermal Engineering*, 30(6-7):760 – 769.

Papadopoulos, A. I., Stijepovic, M., Linke, P., Seferlis, P., and Voutetakis, S. (2013). Toward optimum working fluid mixtures for organic rankine cycles using molecular design and sensitivity analysis. *Ind. Eng. Chem. Res.*, 52(34):12116–12133.

Puth, M.-T., Neuhäuser, M., and Ruxton, G. D. (2015). Effective use of spearman's and kendall's correlation coefficients for association between two measured traits. *Animal Behaviour*, 102:77 – 84.

Quoilin, S., Broek, M. V. D., Declaye, S., Dewallef, P., and Lemort, V. (2013). Techno-economic survey of organic rankine cycle (ORC) systems. *Renewable and Sustainable Energy Reviews*, 22:168 – 186.

Stavrou, M., Lampe, M., Bardow, A., and Gross, J. (2014). Continuous molecular targeting-computer-aided molecular design (CoMT-CAMD) for simultaneous process and solvent design for CO2 capture. *Ind. Eng. Chem. Res.*, 53(46):18029–18041.

Tchanche, B. F., Papadakis, G., Lambrinos, G., and Frangoudakis, A. (2009). Fluid selection for a low-temperature solar organic rankine cycle. *Applied Thermal Engineering*, 29(11-12):2468 – 2476.

Wang, Z. Q., Zhou, N. J., Guo, J., and Wang, X. Y. (2012). Fluid selection and parametric optimization of organic rankine cycle using low temperature waste heat. *Energy*, 40(1):107 – 115.

ACKNOWLEDGEMENT

We thank the Deutsche Forschungsgemeinschaft (DFG) for funding this work (BA2884/4-1).